Journal of Power Sources 238 (2013) 245–250

Contents lists available at SciVerse ScienceDirect

Journal of Power Sources

journal homepage: www.elsevier.com/locate/jpowsour

Short communication

Tailored synthesis of $Ni_{0.25}Mn_{0.75}CO_3$ spherical precursors for high capacity Li-rich cathode materials via a urea-based precipitation method

Jingwen Zhang, Xun Guo, Sumei Yao, Wentao Zhu, Xinping Qiu*

Key Lab of Organic Optoelectronics and Molecular Engineering, Department of Chemistry, Tsinghua University, Beijing 100084, China

HIGHLIGHTS

- ($Ni_xMn_{1-x}CO_3$) is prepared via a urea-based homogeneous precipitation method.
- The work presents the optimized conditions for the preparation of carbonate precursor.
- It gives the nucleation and growth mechanism process of carbonate precursors.
- The obtained powders exhibit good cycling performance.

ARTICLE INFO

Article history:
Received 2 December 2012
Received in revised form
27 February 2013
Accepted 7 March 2013
Available online 26 March 2013

Keywords:
Cathode material
Layered material
Lithium rich material
Tailored synthesis
Precipitation
Lithium-ion battery

ABSTRACT

This study develops a urea-based homogeneous precipitation method to synthesize spherical carbonate precursors ($Ni_{0.25}Mn_{0.75}CO_3$) for the Li-rich layered cathode material $Li(Ni_{0.2}Li_{0.2}Mn_{0.6})O_2$. The structure and morphology of the precursor particles were tailored by controlling of urea concentration, reaction temperature and time. Combined with XRD, SEM, and particle size analysis, the optimized conditions for synthesizing desired stoichiometric $Ni_{0.25}Mn_{0.75}CO_3$ were obtained. We also investigated the processes of nucleation and growth of precursors. The obtained spherical $Li(Ni_{0.2}Li_{0.2}Mn_{0.6})O_2$ delivers discharge capacity of 237 mAh g^{-1} at the initial cycle and 253 mAh g^{-1} after 50 cycles.

1. Introduction

Lithium ion batteries have been regarded as one of promising power source candidates for electric vehicles in recent years [1–3]. However, high price and low energy density are still obstacles for applications of Li-ion batteries in EVs and other renewable energy systems. [4]. Recently, composited lithium and manganese-rich $Li_{1+x}M_{1-x}O_2$ compounds (M = Mn, Ni, Co) have attracted much attention due to their low cost, high capacity (>250 mAh g^{-1}) and structural stability at high voltage (>4.6 V) [5–8]. In preparation of these materials, the precursors play important roles on electrochemical performances of the final products [9,10]. The precursors were usually prepared by hydroxide, carbonate co-precipitation or sol–gel methods [11–15]. However, a major drawback for the hydroxide co-precipitation method is that Mn^{2+} is easily oxidized to Mn^{3+} and causes other phase formation, resulting in impurity phases in final product [16]. The sol–gel method usually requires careful aging and time consuming drying steps, which is unsuitable for large scale production. Carbonate co-precipitation, as an alternative method to prepare precursors of transition metal compounds (Ni, Co, Mn), may keep Mn in divalent oxidation state since the pH value of solution for carbonate co-precipitation is around 8, which is less harsh than that in a hydroxide process (pH = 11) [17], while the serious stirring is needed in the continuous stirred tank reactor [15,18].

In this work, we successfully developed a urea-based homogeneous precipitation method for preparation spherical carbonate precursors of $Ni_xMn_{1-x}CO_3$ ($0 < x < 1$). The decomposition of urea releases precipitating anions (mainly OH^- and CO_3^{2-}) slowly and homogeneously into the reaction systems at elevated temperature, and thus results in the homogeneous precipitation of the precursor

* Corresponding author. Tel./fax: +86 10 62794234.
E-mail addresses: qiuxp@mail.tsinghua.edu.cn, 823406675@qq.com (X. Qiu).

0378-7753/$ – see front matter © 2013 Elsevier B.V. All rights reserved.
http://dx.doi.org/10.1016/j.jpowsour.2013.03.094

particles even without stirring. The conditions that influence the homogeneity, morphology of carbonate precursors, and subsequently the electrochemical performance of the final material ($Li(Ni_{0.2}Li_{0.2}Mn_{0.6})O_2$) were also investigated.

2. Experimental methods

Nickel nitrate hexahydrate ($Ni(NO_3)_2{\cdot}6H_2O$), manganese sulfate monohydrate ($MnSO_4{\cdot}H_2O$), urea ($CO(NH_2)_2$), and lithium carbonate (Li_2CO_3) were used as the starting materials. The precursors were prepared as follows: $Ni(NO_3)_2{\cdot}6H_2O$ and $MnSO_4{\cdot}H_2O$ (cationic ratio of Ni:Mn = 1:3) were dissolved in de-ionized water to form 1 mmol L^{-1} solution. At the same time, some amount of urea was added under rigorous stirring to form a clear mixed solution. Then the mixed solution was transferred into a Teflon-lined stainless steel autoclave and reacted at an elevated temperature for a period of time. In this study, 12 precursor samples were prepared with various urea concentration, reaction time and temperature, as listed in Table 1. Collected products were filtered, washed, and dried at 100 °C over 24 h. The obtained precursors and Li_2CO_3 were mixed thoroughly, heated at 500 °C for 5 h and at 900 °C for 24 h in air, then quenched in air to obtain final products.

The structure characterization with X-ray diffraction (XRD) was conducted on a D8 Advance Bruker diffractometer, using a Cu-Kα radiation source (λ = 1.5406 Å). The morphology of the materials was observed by a Hitachi S-4500 scanning electron microscope (SEM). The element distributions on the internal cross section of the prepared carbonate and calcinated lithiated particles were analyzed by an electron-probe micro-analyzer (Hitachi S-6301). The particle size was measured via a Laser Particle Size Analyzer (Mastor 2000), and the composition of the filtrates was measured by an Inductively Coupled Plasma Optical Emission Spectrometer (ICP-OES, IRIS Intrepid II).

The electrode foil for electrochemical tests consisted of 85 wt% active material, 5 wt% poly(vinylidene fluoride) as binder, and 10 wt % carbon black as conducting agent. After being blended in *N*-methylpyrrolidinone, the slurry was casted uniformly onto aluminum foil and dried at 80 °C for 12 h in vacuum. A typical electrode contained active material of 3–4 mg cm^{-2}. Charge and discharge performance was evaluated using 2025 coin cells containing an electrolyte solution of 1 M $LiPF_6$ in a mixed solvent of ethylene carbonate (EC) and dimethyl carbonate (DMC) (1:1 volume ratio) with Celgard 2320 micro-porous membrane as separator. Metallic lithium foil served as the counter electrode. The cells were assembled in an argon-filled glove-box (O_2 and H_2O levels <1 ppm). Galvanostatic charge and discharge were controlled between 2.0 and 4.8 V at a constant current density of 20 mA g^{-1} at room temperature (Xinwei CT3008W, Shenzhen Xinwei Electronic Co, China).

3. Results and discussion

3.1. Preparation of the carbonate precursors

In the process of preparing precursors, the precipitation agent of urea serves as a reservoir for precipitating anions. X-ray diffraction patterns of precursors with different reaction time are shown in Fig. 1. The typical diffraction peaks of MCO_3 (M = Ni and Mn) can be seen. Weak reflections at 2θ = 12.3° and 18.3°, which may be assigned to NiOOH and $Mn(OH)_2$, can be found at the beginning of the reaction and disappeared after 1.0 h, meaning that competitive reactions between the hydroxide and carbonate co-precipitation exist due to the fluctuation of OH^- and CO_3^{2-} concentrations inside the reactor. When the CO_3^{2-} concentration stabilized, carbonate precursor particles formed. Before 2.0 h there were only peaks indexed to $MnCO_3$; as time elapses, the $NiCO_3$ peaks became more clearly (Fig. 1), in agreement with the residual transition metal concentration in solution (Table 1).

The SEM images (as shown in Fig. 2) reveal the processes of particle nucleation and growth during the co-precipitation. After 30 min of reaction, the particles are composed of loose agglomerates with no defined shape, and the maximum particle size distribution is at 4.47 μm (Fig. 3(a), 0.5 h). When the time was up to 1.0 h, spherical particles appeared (Fig. 2(b), 1.0 h). As the time is longer than 2.0 h, the collected particles, composed of nano-sized primary particles, are all with spherical morphology. These SEM observations are in accordance with the particle size distribution results in Fig. 3. The particle size distributions of samples collected from 2.0 h to 12 h are narrow slightly, and two small peaks appear below 5 μm, possibly due to disintegration of the large particles. The distribution maximum is at 4.47 μm (0.5 h), 22.44 μm (1.0 h), 21.22 μm (2.0 h), 26.72 μm (4.0 h), 26.72 μm (6.0 h), and 23.81 μm (12 h), respectively. The internal cross section and the line scanning of Ni and Mn are shown in Fig. 4. The diameter of the selected spherical particle is about 33 μm, the contents of the transition metal elements (Ni & Mn) are constant inside the particle. On the surface, the Ni content increased abruptly which is in agreement with results of XRD (Fig. 1(d)–(f)) and the residual transition metal concentration in solution (Table 1). Based on this phenomenon, we assumed that Ni^{2+} and Mn^{2+} may co-precipitate at the beginning of the reaction; as

Table 1
Synthetic conditions of carbonate precursor particles.

Sample	Temperature (°C)	Urea concentration n(urea) / n(Ni+Mn)	Time (hour)	Average particle size (D50,μm)	The residual transition metal concentration in solution	
					Mn (mg L^{-1})	Ni (mg L^{-1})
P1	200	2.0 : 1.0	0.5	4.76	8536	4196
P2	200	2.0 : 1.0	1.0	15.36	147.4	949.4
P3	200	2.0 : 1.0	2.0	29.62	0.4302	825.6
P4	200	2.0 : 1.0	4.0	27.39	0.1988	368.3
P5	200	2.0 : 1.0	6.0	26.67	0.2012	84.68
P6	200	2.0 : 1.0	12	24.10	0.1363	73.37
P7	100	2.0 : 1.0	6.0	18.29	5681	3563
P8	140	2.0 : 1.0	6.0	31.05	0.9370	1858
P9	180	2.0 : 1.0	6.0	25.81	0.2209	392.5
P10	200	0.5 : 1.0	6.0	5.75	4896	1658
P11	200	1.0 : 1.0	6.0	11.51	285.0	1193
P12	200	4.0 : 1.0	6.0	22.60	0.2049	112.7

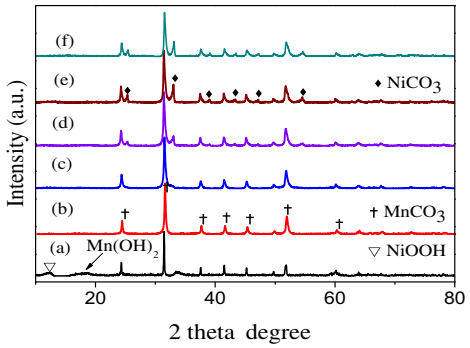

Fig. 1. XRD patterns of precursor samples collected after different reaction time: (a) 0.5 h, (b) 1.0 h, (c) 2.0 h, (d) 4.0 h, (e) 6.0 h and (f) 12 h (Table 1 provided the synthetic conditions in detail).

time elapses, the particle formed were less homogeneous in chemical composition as a result of the more residual Ni^{2+} in solution. The process of particle growth is shown in schematic illustration (Fig. 5). The agglomeration was likely due to the surface tension or electrostatic force between the seed particles (Fig. 2(b)) [15].

Co-precipitation via a urea-based homogeneous precipitation method is a complicated process. Besides the reaction time, temperature should be well controlled. The temperatures during the precipitation process were selected as 100 °C, 140 °C, 180 °C and 200 °C, respectively. X-ray diffraction is shown in Fig. S1. It can be seen that the main component of the precipitates was carbonates; however, at 100 and 140 °C, the peaks were consistent with the formation of $MnCO_3$, indicating that there were less nickel elements in the precipitate particles. By increasing the reaction temperature to 180 °C, mixture of $MnCO_3$ and $NiCO_3$ can be found, and the intensity of the $NiCO_3$ peaks increased at 200 °C. On the other hand, the residual transition metal concentrations in solution decreased with increasing temperature (Table 1). During precipitation, $MnCO_3$ was precipitated firstly because the decomposition of urea was slower at lower temperature and the equilibrium constant of $MnCO_3$ ($K_{sp} = 4.27 \times 10^{10}$) is much higher than that of $NiCO_3$ ($K_{sp} = 7.04 \times 10^{6}$). The shape of the secondary particles was all spherical and the size of primary particles (square shape) increased from 100 nm (P7) to 400 nm (P9 & P5), when the temperature was increased from 100 °C to 200 °C.

The decomposition of urea releases not only precipitating anions (mainly OH^- and CO_3^{2-}) into the reaction systems, but also NH_4^+, which is the source of NH_3, and NH_3 can react with M^{2+} (M = Ni and Mn) to produce $[M(NH_3)_n]^{2+}$ complexes. In addition, M^{2+} ions and $[M(NH_3)_n]^{2+}$ complexes are considered as the residual species in the solution (M = Ni and Mn) [19]. Thus, to minimize

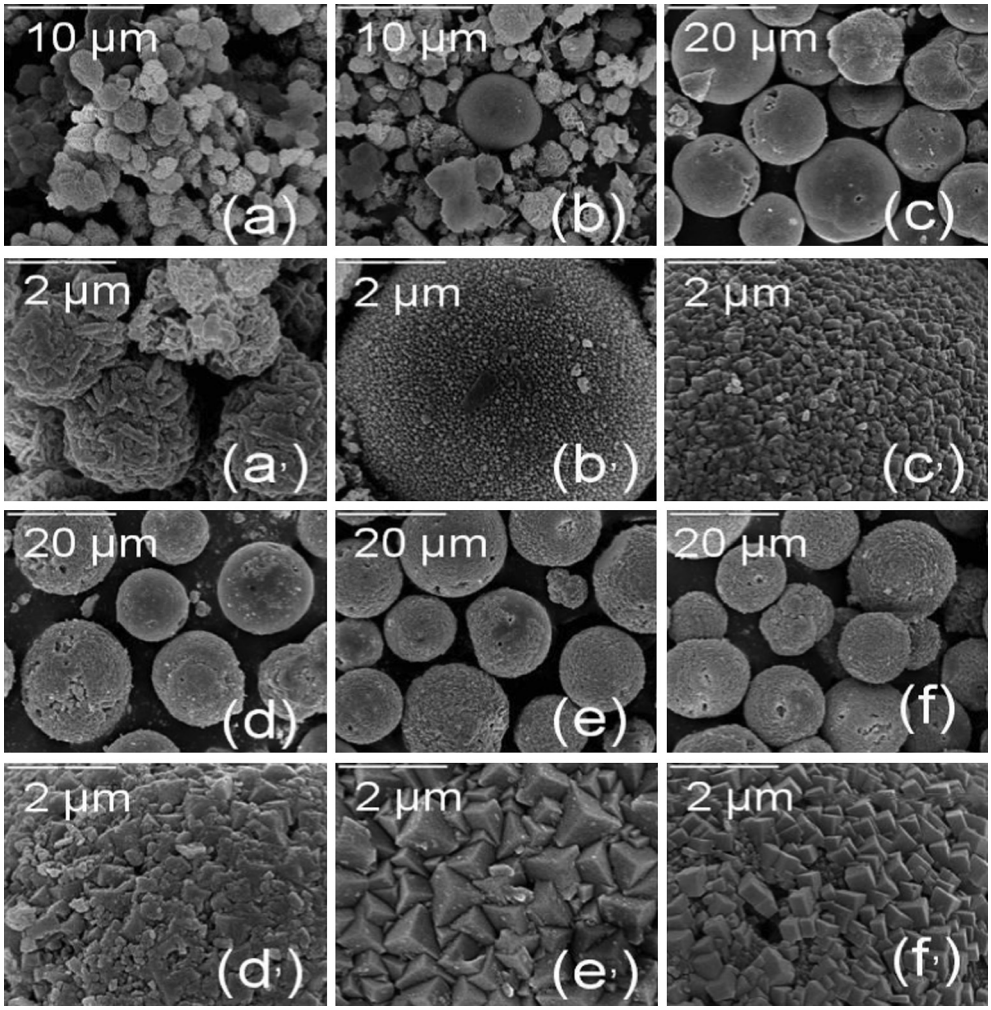

Fig. 2. SEM images and particle distributions of samples collected at different urea concentration: (a) 0.5 h, (b) 1.0 h, (c) 2.0 h, (d) 4.0 h, (e) 6.0 h and (f) 12 h (Table 1 provided the synthetic conditions in detail).

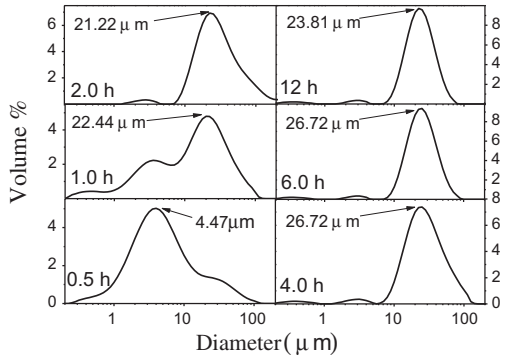

Fig. 3. Particle distributions of samples collected at different reaction time: (a) 0.5 h, (b) 1.0 h, (c) 2.0 h, (d) 4.0 h, (e) 6.0 h and (f) 12 h (Table 1 provided the synthetic conditions in detail).

the residual transition metal concentration in solution is necessary to prepare stoichiometric precursor with the desired transition metal ratio. It means that the amounts of urea must to be well controlled, which were described in Table 1 (sample P10, P11, P5 & P12). When the molar ratio of urea to transition metals (Ni and Mn) was 0.5:1.0 (sample P10), both of NiOOH and $Mn(OH)_2$ were observed in the XRD pattern (Fig. S3(a)) besides $MnCO_3$. But the NiOOH and $Mn(OH)_2$ peaks became lower for the sample P11, which finally disappeared at the ratio of 2.0:1.0. At the low urea concentration (molar ratio, 0.5:1.0), the NiOOH and $Mn(OH)_2$ peaks were observed because there were less CO_3^{2-} than the transition metals, and the NiOOH is thermodynamically much more stable than $NiCO_3$. Therefore, as the molar ratio increased (up to 2.0:1.0), the CO_3^{2-} concentration, released by urea at elevated temperature, is high enough for the precipitation of transition metal ions. However, when the urea ratio increase to 4.0:1.0, more $[Ni(NH_3)_n]^{2+}$ is left in solution, the stoichiometry of the precursor may distort. In this work, the optimized molar ratio of urea and transit metal were obtained at 2.0:1.0.

3.2. Electrochemistry of the synthesized $Li(Ni_{0.2}Li_{0.2}Mn_{0.6})O_2$ powders

To prepare stoichiometric precursor with the desired transition metal ratio, the precursors must be collected after 6.0 h of carbonate co-precipitation. So the precursor P5 was used to prepare $Li(Ni_{0.2}Li_{0.2}Mn_{0.6})O_2$. The XRD pattern of final product of $Li(Ni_{0.2}Li_{0.2}Mn_{0.6})O_2$ was primarily indexed based on the *Rm* space group, which is the structure of the major layered component in similar materials (Fig. 6). Some weak peaks between 20° and 25° of 2θ can be observed in the XRD patterns, which are considered to be caused by the short-range super-lattice ordering of Li, Ni, Mn in the transition metal layer. These peaks can be indexed to C2/*m* space group that characterizes Li_2MnO_3 [20–22]. Fig. 7(a) shows the morphology of $Li(Ni_{0.2}Li_{0.2}Mn_{0.6})O_2$ particles. It can be seen that the morphology of the secondary particles maintains spherical shape and the size of particle shrinks a little though the primary particles is with no defined shape and sintered each other. After the calcination at high temperature, the Ni-rich layer on the particle surface became less obvious (as shown in Fig. 7(b) and (c)) due to diffusion of Ni & Mn.

The first and second charge–discharge profiles of $Li(Ni_{0.2}Li_{0.2}Mn_{0.6})O_2$ is shown in Fig. 8. The cell was initially charged to 4.8 V, discharged to 2.0 V and then cycled between 2.0 and 4.8 V in the subsequent cycles at current density of 20 mA g^{-1}. The initial charging curves show two plateaus: one is observed below 4.5 V, and the other is above 4.5 V. At the former plateau, the voltage increases monotonically, corresponding to the oxidation of Ni^{2+} to Ni^{4+}, until the potential reaches 4.5 V, and the latter results from the electrochemical removal of 'Li_2O' from the structure, correlating with the activation of Li_2MnO_3, which is responsible for the large irreversible capacity in the first cycle. The irreversible capacity disappeared in the second and subsequent cycles, in agreement with the literature reports [23–26].

The cycle life of samples prepared from different precursors is compared in Fig. 9. According to the serial number of precursors, the final products are named as S_{P5}, S_{P7}, S_{P8}…. Fig. 9(a) illustrates the cycling performance of samples prepared from precursor P7, P8,

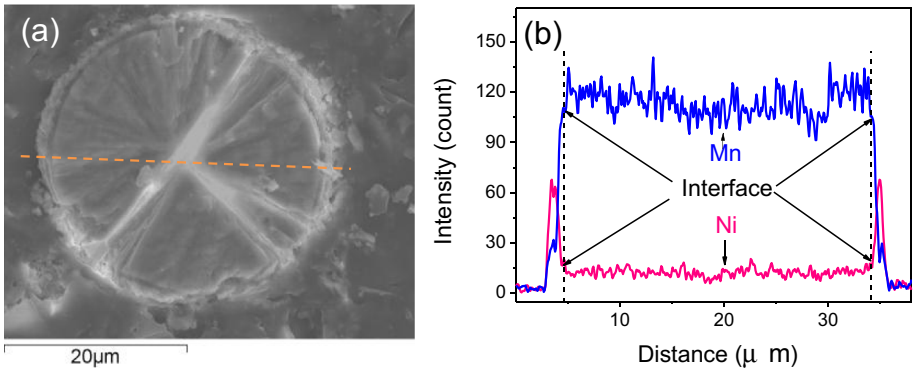

Fig. 4. Scanning electron microscopy (SEM) and electron-probe X-ray micro-analysis (EPMA) results for the sample collected at 6.0 h: (a) SEM photograph and (b) EPMA line scan.

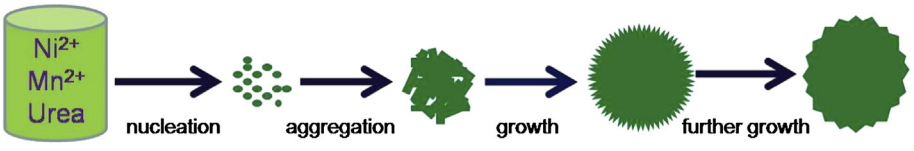

Fig. 5. Schematic illustration for the overall formation process of microspheres.

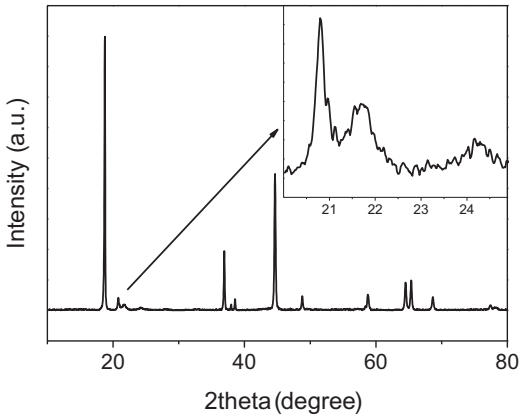

Fig. 6. X-ray diffraction patterns of $Li(Ni_{0.2}Li_{0.2}Mn_{0.6})O_2$ and enlarged section between 20° and 25° of 2 theta.

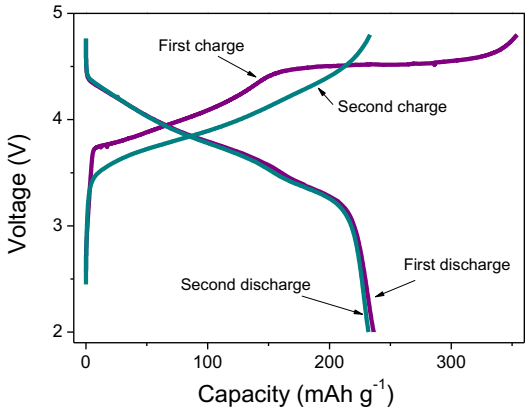

Fig. 8. The first and second charge–discharge profiles of $Li(Ni_{0.2}Li_{0.2}Mn_{0.6})O_2$.

P9 and P5, which were synthesized under different temperatures (100 °C, 140 °C, 180 °C and 200 °C). The discharge capacity of S_{P7} was only 161 mAh g^{-1} in the first cycle, and then increased to 220 mAh g^{-1} after 30 cycles. When the temperature of precursor preparation was increased to 140 °C, the discharge capacity of S_{P8} was maintained at about 228 mAh g^{-1} exhibiting good cycling performance. However, the capacity was still lower than that of S_{P9} and S_{P5}, whose precursors were collected at 180 °C and 200 °C respectively. That may be because urea cannot decompose completely at lower temperature and more nickel elements are remained in solution (as shown in Table 1 column 7), resulting in the lower nickel content in S_{P7}. Fig. 9(b) illustrates the cycling performance of samples prepared from precursor P10, P11, P5 and P12, which were synthesized under different urea concentration. The final products (S_{P10}, S_{P11}, S_{P5} and S_{P12}) had different discharge capacities. At the low urea concentration (molar ratio, 0.5:1.0), the CO_3^{2-} released by urea is not enough for the precipitation of transition metal ions (especially for Ni^{2+}). However, when the urea ratio increase to 4.0:1.0, more $[Ni(NH_3)_n]^{2+}$ is left in solution, the stoichiometry of the final products may distort. Based on the analysis above, the synthetic conditions for precursors must be well controlled to prepare stoichiometric product with the desired elements ratio.

In this work, the optimized condition to prepare stoichiometric carbonate precipitation is at 200 °C for 6 h when the molar ratio of

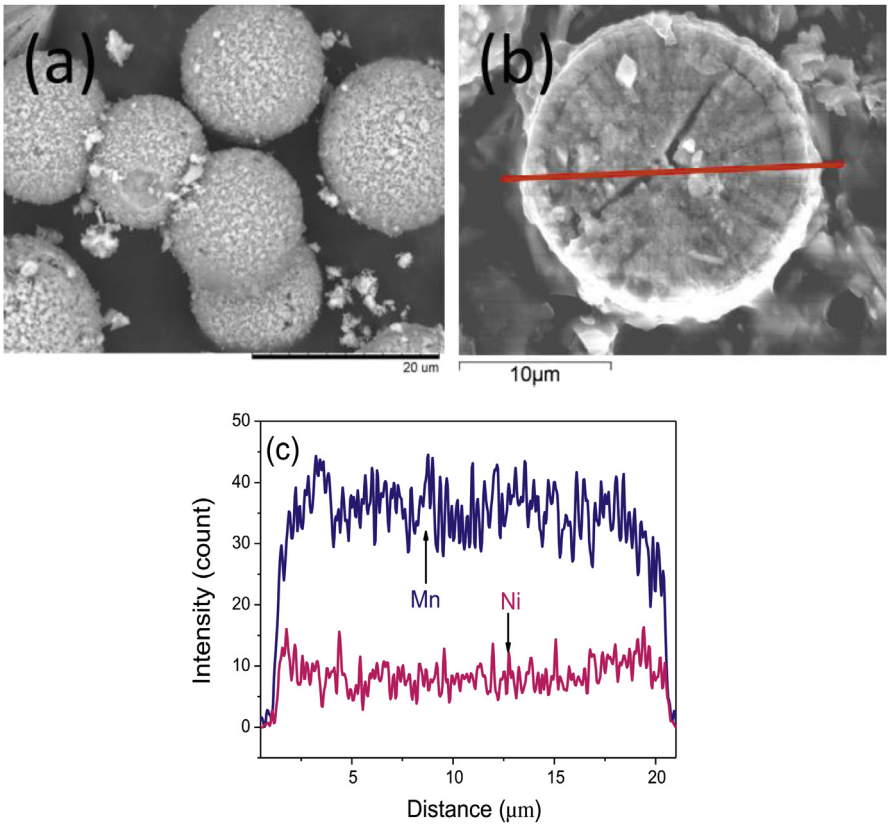

Fig. 7. SEM image of sample calcined at 900 °C: (a) secondary particles, (b) the polished surface and (c) EPMA line scan.

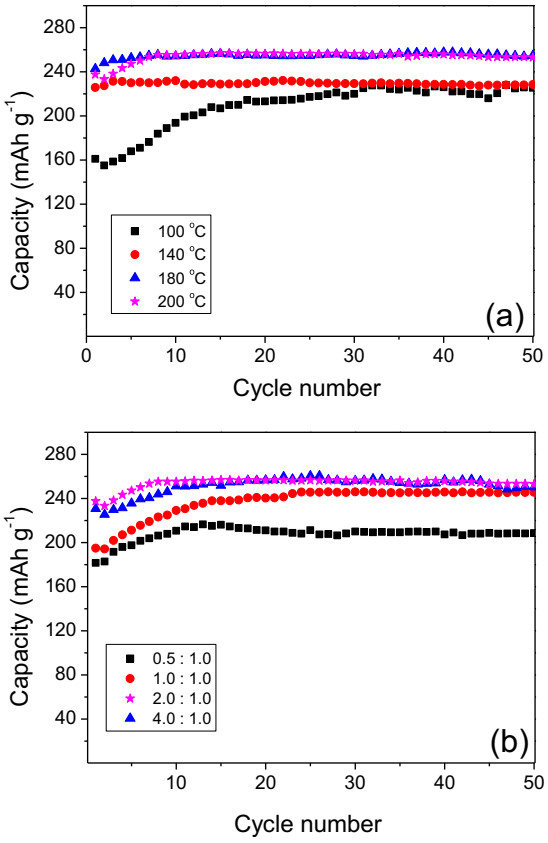

Fig. 9. The cycle performance of samples prepared from different precursors, which were synthesized at: (a) different temperatures & (b) different urea concentrations (Table 1 provided the synthetic conditions in detail).

urea and transition metal is 2.0:1.0. The corresponding sample S_{P5} ($Li(Ni_{0.2}Li_{0.2}Mn_{0.6})O_2$) had a discharge capacity of about 237 mAh g^{-1} at the initial cycle, and the reversible capacity was also 253 mAh g^{-1} after the 50th charge–discharge cycles, exhibiting good cycling performance (shown in Fig. 9). However, the large particle size is possibly disadvantageous to the lithium diffusion, which led to electrochemically inactivated core. Therefore, further studies must be made to produce smaller particle powders, promoting the lithium diffusion and improving the capacity of $Li(Ni_{0.2}Li_{0.2}Mn_{0.6})O_2$.

4. Conclusions

In summary, this study introduces a urea-based homogeneous precipitation method to synthesize carbonate precursors ($Ni_{0.25}Mn_{0.75}CO_3$) for the Li-rich layered cathode material $Li(Ni_{0.2}Li_{0.2}Mn_{0.6})O_2$, and the structure and morphology of the precursor particles were tailored by controlling the urea concentration, reaction temperature and time. Combined with XRD, SEM, and particle size analysis, the optimized conditions to attain desired stoichiometric $Ni_{0.25}Mn_{0.75}CO_3$ were confirmed as 200 °C, 6 h, and the molar ratio of urea to transition metals (Ni and Mn) of 2.0:1.0. The nucleation and growth process began with the formation of a mixture of carbonate salts and hydroxide impurities, and the impure phases disappeared with time. The reaction started with the formation of seeds with no defined shape, continued with the growing of these small particles, and ended with the production of spherical, homogeneous particles (average particle size was 26.67 μm) with the transition metal ratio close to that of the reactants. The synthesized powders of $Li(Ni_{0.2}Li_{0.2}Mn_{0.6})O_2$ had a mixture of layered structure with the *Rm* and C2/*m* symmetry. The obtained powders had a discharge capacity of about 237 mAh g^{-1} at the initial cycle, and the reversible capacity was also 238 mAh g^{-1} at the 50th cycle, exhibiting good cycling performance.

Acknowledgment

The authors appreciate the financial support from State Key Basic Research Program of PRC (2009CB220105, 2013CB934000), Beijing Natural Science Foundation (2120001), National Natural Science Foundation of China (21273129), National International Science and Technology Cooperation Project (2012DFG61480), 863 (2011AA11A290), and China–US Electric Vehicle Project (2010DFA72760).

Appendix A. Supplementary data

Supplementary data related to this article can be found at http://dx.doi.org/10.1016/j.jpowsour.2013.03.094.

References

[1] J.Y. Kim, D.Y. Lim, Energies 3 (2010) 866.
[2] F.Y. Cheng, Z.L. Tao, J. Liang, J. Chen, Chem. Mater. 20 (2008) 667.
[3] M.S. Whittingham, Chem. Rev. 104 (2004) 4271.
[4] I. Belharouak, W. Lu, D. Vissers, K. Amine, Electrochem. Commun. 8 (2) (2006) 329.
[5] A. Abouimrane, O.C. Compton, H.X. Deng, I. Belharouak, D.A. dikin, S.T. Neguyen, K. Amine, Electrochem. Solid State Lett. 14 (9) (2011) A126.
[6] M.G. Kim, M. Jo, Y.S. Hong, J. Cho, Chem. Commun. 2 (2009) 18.
[7] L. Croguennec, J. Bains, M. Ménétrier, A. Flambard, E. Bekaert, C. Jordy, P. Biensan, C. Delmas, J. Electochem. Soc. 156 (5) (2009) A349.
[8] J. Gao, J. Kim 1, A. Manthiram, Electrochem. Commun. 11 (2009) 84.
[9] K. Lee, S. Myung, J. Moon, Y. Sun, Electrochim. Acta 53 (2008) 6033.
[10] H. Bang, B. Park, J. Prakash, Y. Sun, J. Power Sources 174 (2007) 565.
[11] C.S. Johnson, N. Li, C. Lefief, M.M. Thackeray, Electrochem. Commun. 9 (2007) 787.
[12] Y.K. Sun, M.G. Kang, S.H. Kang, K. Amine, Electrochem. Solid State Lett. 13 (2003) 319.
[13] H. Deng, I. Belharouak, C.S. Yoon, Y.-K. Sun, K. Amine, J. Electochem. Soc. 157 (10) (2010) A1035.
[14] H. Deng, I. Belharouak, Y.K. Sun, K. Amine, J. Mater. Chem. 19 (2009) 4510.
[15] D.P. Wang, I. Belharouak, G.M. Koenig, G.W. Zhou, K. Amine, J. Mater. Chem. 21 (2011) 9290.
[16] F. Zhou, X.M. Zhao, A. Bommel, A.W. Rowe, J.R. Dahn, Chem. Mater. 22 (2010) 1015.
[17] M.H. Lee, Y.J. Kang, S.T. Myung, Y.K. Sun, Electrochim. Acta. 50 (2004) 939.
[18] G. Jia, M. Yang, Y.H. Song, H.P. You, H.J. Zhang, Cryst. Growth Des. 9 (1) (2009) 301–307.
[19] A.V. Bommel, J.R. Dahn, Chem. Mater. 21 (2009) 1500.
[20] M.M. Thackeray, S.H. Kang, C.S. Johnson, J.T. Vaughey, R. Benedek, S.A. Hachney, J. Mater. Chem. 17 (2007) 3112.
[21] M.M. Thackeray, C.S. Johnson, J.T. Vaughey, N. Li, S.A. Hachney, J. Mater. Chem. 17 (2007) 2069.
[22] S.K. Kang, P. Kempgens, S. Greenbaum, A.J. Kropf, K. Amine, M.M. Thackeray, J. Mater. Chem. 15 (2005) 2257.
[23] B. Ammundsen, J. Paulsen, Adv. Mater. 13 (2001) 943.
[24] N. Yabuuchi, K. Yoshii, S.T. Myung, I. Nakai, S. Komaba, J. Am. Chem. Soc. 133 (2011) 4404.
[25] C.S. Johnson, J.S. Kim, C. Lefief, N. Li, J.T. Vaughey, M.M. Thackeray, Electrochem. Commun. 8 (2004) 1085.
[26] A.D. Robertson, P.G. Bruce, Electrochem. Solid State Lett. 7 (9) (2004) A294.